Radiation Physics and Chemistry 223 (2024) 111974

Contents lists available at ScienceDirect

Radiation Physics and Chemistry

journal homepage: www.elsevier.com/locate/radphyschem

Experimental design of size variation in albumin nanoparticles synthesized by electron beam

Aryel H. Ferreira [a,b,c,1,*], Caroline S.A. Lima [a,b,1,**], Cassia Priscila Cunha da Cruz [b], Lucas F. Freitas [a,b], Gustavo N. Furlan [d,e], Robson C. de Lima [d,e], Gabriel Adrián Sarriés [d,e], Ademar B. Lugão [b]

[a] MackGraphe - Mackenzie Institute for Research in Graphene and Nanotechnologies, Mackenzie Presbyterian University, Sao Paulo, 01302-907, Brazil
[b] Nuclear and Energy Research Institute, IPEN-CNEN/SP, Sao Paulo, 05508-000, Brazil
[c] Mackenzie Evangelical College of Paraná - Mackenzie Presbyterian University, Curitiba, PR, 80730-000, Brazil
[d] College of Agriculture Luiz de Queiroz, University of São Paulo, Piracicaba, 13418-900, Brazil
[e] Nuclear Energy Center for Agriculture, University of São Paulo, Piracicaba, 13416-000, Brazil

ARTICLE INFO

Handling Editor: Piotr Ulanski

Keywords:
Albumin nanoparticle
Electron beam irradiation
One-step synthesis
Protein crosslinking

ABSTRACT

Protein-based nanoparticles have garnered significant interest for their potential in theranostic applications, including cancer treatment and nuclear medicine. Plasma proteins are particularly appealing due to their ability to bypass the rapid clearance typically associated with synthetic particles. Human serum albumin (HSA), for example, is already utilized in diagnostic procedures such as lymphoscintigraphy and sentinel lymph node detection and in cancer treatments where it delivers therapeutic agents in nanoparticulate form. Among the various techniques for synthesizing protein nanoparticles, ionizing radiation stands out for its ability to maintain good size control and preserve the protein's three-dimensional structure. Factors such as the reaction precursor, pH, protein concentration, presence of a stabilizer, and irradiation dose can all influence the size and shape of the resulting nanoparticles. This study sought to identify a correlation between the size of albumin nanoparticles and reaction parameters, including protein concentrations, the ionic content of the buffer solution, and the e-beam irradiation dose. We conducted different synthesis methods with varying BSA concentrations, using two different buffers and varying radiation doses. The resulting nanoparticles were evaluated using Dynamic Light Scattering. The size data were statistically analyzed using SAS Studio, SAS JMP, and WEKA software to identify correlations among the synthesis variables. Our observations primarily revealed that lower protein concentrations consistently resulted in smaller particles. Additionally, using Tris-HCl buffer as a medium led to a more proportional growth of particles with increases in concentration and irradiation dose. These findings suggest that Tris buffer is more suitable for BSA nanoparticle synthesis, as increased albumin concentration and radiation dose resulted in more consistent size control.

1. Introduction

The development of protein-based nanoparticles as vehicles for therapeutic molecules and radionuclides represents an excellent opportunity in oncology and nuclear medicine. The advantages of using proteins to synthesize these systems include the abundance of proteins extracted from natural sources, biocompatibility, biodegradability, and a relatively easy synthesis process, unlike other systems that use metals and other inorganic and synthetic materials (Verma et al., 2018). Furthermore, the profusion of hydroxyl-, amino-, and carboxyl groups present in protein nanoparticles offers the possibility of surface modification by conjugating ligands such as peptides, proteins,

* Corresponding author. MackGraphe - Mackenzie Institute for Research in Graphene and Nanotechnologies, Mackenzie Presbyterian University, Sao Paulo, 01302-907, Brazil.
** Corresponding author. MackGraphe - Mackenzie Institute for Research in Graphene and Nanotechnologies, Mackenzie Presbyterian University, Sao Paulo, 01302-907, Brazil.
E-mail addresses: aryel.ferreira@mackenzie.br (A.H. Ferreira), caroline.lima@alumni.usp.br (C.S.A. Lima).
[1] These authors contributed equally.

https://doi.org/10.1016/j.radphyschem.2024.111974
Received 6 November 2023; Received in revised form 2 April 2024; Accepted 21 June 2024
Available online 24 June 2024

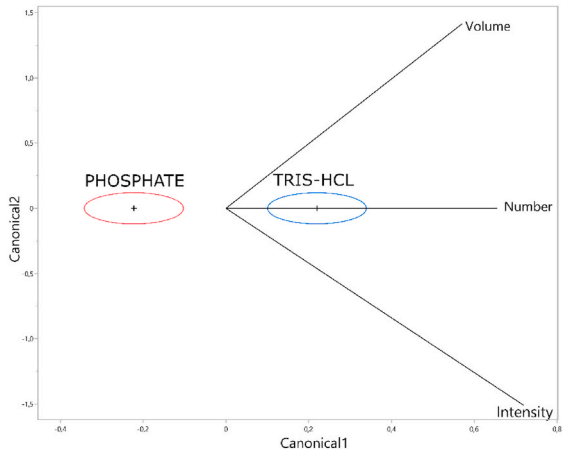

Fig. 1. Plot of canonical variables, derived from linear discriminant analysis, which allows a reduction in dimension and indicates the difference between the two categories (Phosphate and Tris-HCL) and which variables have greater discriminatory power.

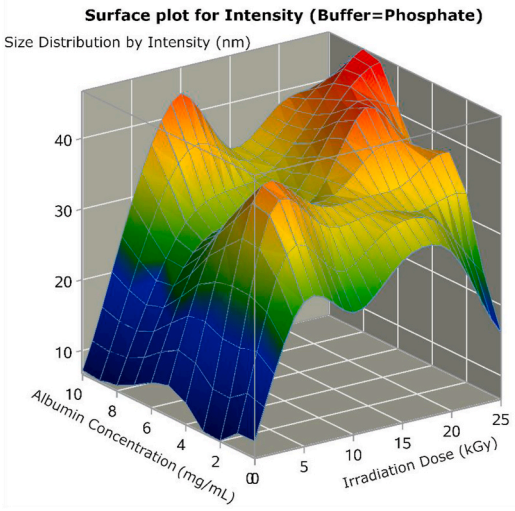

Fig. 2. Surface response plot for albumin nanoparticle size (DLS readings by intensity) considering synthesis conditions in phosphate buffer (pH 7.4), according to protein concentration variation (from 0.5 to 10 mg/mL) and irradiation dose variation (from 1 to 25 kGy).

carbohydrates, antibodies, and drugs via covalent or intermolecular bonds, leading to a more controlled delivery to target tissues and organs and, consequently, further reducing systemic toxicity (Jain et al., 2018; Varca et al., 2016).

The scientific community has explored the potential of several proteins from animals and plants, such as albumin, gelatin, and fibroin (Lohcharoenkal et al., 2014); using protein nanoparticles for biotechnological applications is already a reality. They have become an alternative to improve the pharmacokinetics and pharmacodynamic properties of several drugs and radiopharmaceuticals. Depending on the protein characteristics, nanoparticulate systems can be administered by several routes, including oral, intravenous, inhalation, or subcutaneous administration.

The main examples of protein-based nanomedicines approved by the FDA are Abraxane® (consisting of paclitaxel encapsulated in albumin nanoparticles (130 nm), for the treatment of metastatic breast cancer (2005), lung cancer (2012), and metastatic pancreatic adenocarcinoma (2013)); Ontak® (a recombinant protein from diphtheria toxin, called denileukin diftitox, fused to human interleukin-2, indicated for the treatment of relapsed or refractory cutaneous T-cell lymphoma); and Rebinyn® (a drug based on pegylated human recombinant Factor IX for the hemophilia treatment) (Farjadian et al., 2019).

More specifically, albumin is the most abundant plasma protein. It plays many crucial functions, including regulating blood pH, maintaining circulating plasma volume, and modulating the distribution of fluids between body compartments. Furthermore, albumin is involved in transporting endogenous and exogenous compounds such as lipophilic molecules of fatty acids, hormones, metal ions, peptides, proteins, and drugs, increasing its bioavailability and stability in biological fluids (Fanali et al., 2012).

The clinical use of albumin was established during World War II, with its successful application in replacing blood transfusion in wounded soldiers; likewise, studies in 1944 describe the benefits of using albumin to treat cirrhosis (Parodi et al., 2019). As a raw material for the nanocarriers manufacture, albumin is stable under physiological conditions (the biological half-life is about three weeks), in the presence of solvents, and heterogeneous pHs. Due to their natural properties, endogenous and exogenous molecule carriers can be combined with therapeutic, diagnostic, or theranostic agents to improve pharmacokinetics (Parodi et al., 2019).

Currently, BSA is widely used in nuclear medicine radiolabeled with ^{99m}Tc for diagnostic purposes, e.g., blood pool, pulmonary, hepatic, renal, bone marrow scintigraphy, and lymphoscintigraphy depending on its radiopharmaceutical presentation in freeze-dried kits (Zolle, 2007). Specifically, it is used for sentinel lymph node staging in nanoparticulate form.

Several routes are used in protein nanoparticle synthesis. The main ones include desolvation, emulsification, and thermal gelling. Other techniques have been described, such as solvent evaporation and spray drying (Elzoghby et al., 2012). Depending on the application, the method must be optimized to achieve properties of interest, such as improving the effectiveness from the point of view of biocompatibility and particle size control.

In particular, the desolvation technique has been improved and shows good reproducibility in particle size distribution. This method is based on the use of cosolvents (ethanol, methanol, acetone) to promote protein aggregation, and a crosslinking agent responsible for covalently linking them and promoting nanoparticle formation. However, if not correctly removed, crosslinking agent residues can induce undesirable reactions and toxicity to biological systems (Gustavo H.C. Varca et al., 2016).

On the other hand, recent studies using an alternative method based on the crosslinking induced by ionizing radiation led to good size control of nanoparticles with bioactivity and preserved three-dimensional structural characteristics for biomedical applications (Soto Espinoza et al., 2012). The synthesis of radiation-induced nanoparticles in aqueous solution occurs mainly through free radicals generated from water radiolysis. The exposure of proteins to these species causes conformational changes leading the protein to oxidative stress conditions that may lead to the formation of bityrosine bonds, considered one of the primary bonds involved in protein crosslinking (Fazolin et al., 2018). This method has advantages over the conventional ones, as it leads to the sterilization of the flasks' contents simultaneously with the synthesis reaction, and the absence of crosslinking agents guarantees low residual toxicity and reduces possible purification stages of remaining monomers (Queiroz et al., 2016). This type of technology is independent of temperature, as it can be performed in different conditions with satisfactory results. Another advantage resides in the fact that the synthesis with ionizing radiation allows the production of nanomaterials on large scale, meaning that they can be easily scaled up (Čubová and Čuba, 2020).

In this method, size and shape can be tailored by the nature and concentration of the precursors in the reaction and by controlling pH, dose rate, and the presence of a stabilizer. In the case of electron beam (e-beam) radiation, the process usually takes a few minutes. Previous

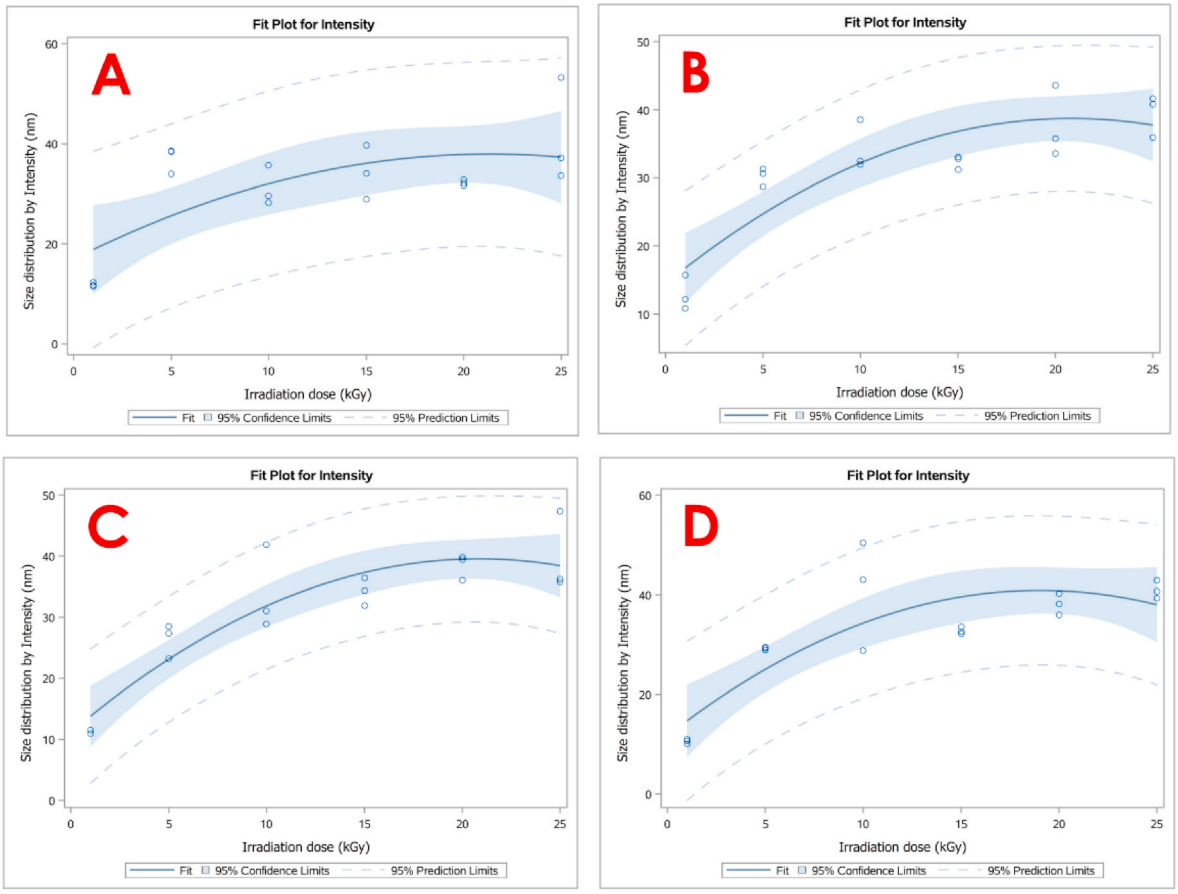

Fig. 3. Regression data of albumin nanoparticle size by means of DLS intensity, according to the irradiation dose (from 1 to 25 kGy) with fixed albumin concentrations of (A) 2.5 mg/mL, (B) 5.0 mg/mL, (C) 7.5 mg/mL, and (D) 10 mg/mL. Data obtained by the synthesis in phosphate buffer.

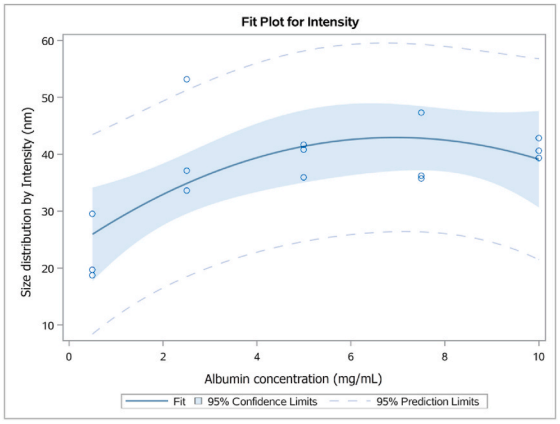

Fig. 4. Increase of albumin nanoparticle size by means of intensity, according to the albumin concentration when the synthesis was performed under fixed irradiation of 25 kGy of in phosphate buffer.

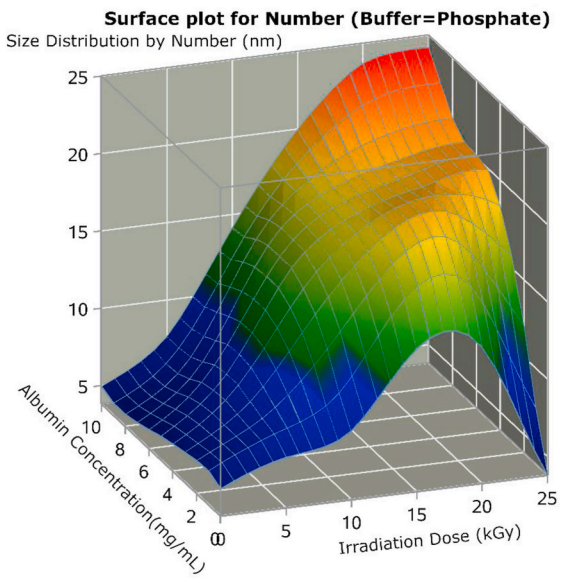

Fig. 5. Size by number surface response plot for albumin nanoparticles synthesized in phosphate buffer, varying protein concentration (from 0.5 to 10 mg/mL) and irradiation dose (from 1 to 25 kGy).

studies suggest that, for example, increasing the dose rate leads to the formation of smaller particles with narrow size distribution (Čubová and Čuba, 2020; Remita et al., 2005).

The convenience of using radiation processing technology is related to its energy efficiency, in which high-energy particles transfer their energy when penetrating the material, allowing reactions to occur at room temperature. These reactions can usually happen without other agents, ensuring the purity of final products, which is vital to prevent toxicity and deterioration of their properties. It is noteworthy that, in terms of technical and safety aspects, e-beam radiation technology is considered better than γ-ray irradiation.

The high-energy e-beam is generated from an electron accelerator.

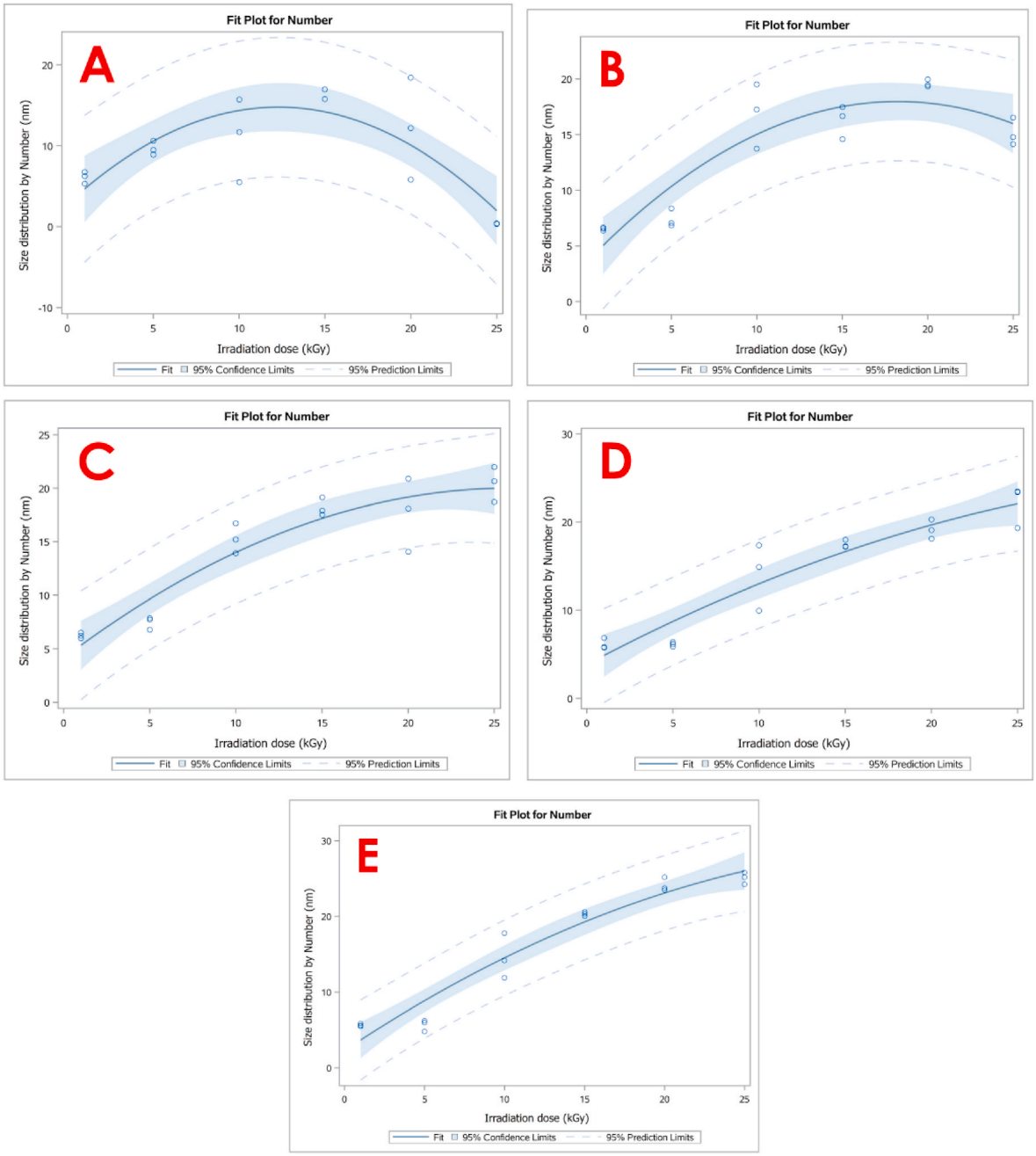

Fig. 6. Regression data of albumin nanoparticle size by number according to the irradiation dose (from 1 to 25 kGy) with fixed albumin concentrations of (A) 0.5 mg/mL, (B) 2.5 mg/mL, (C) 5 mg/mL, and (D) 7.5 mg/mL and (E) 10 mg/mL. Data for the synthesis in phosphate buffer.

When these high-energy electrons penetrate matter, they transfer a small portion of their energy and exit the penetrated object with reduced energy. The higher the initial electron energy, the higher the penetration capacity into matter. Nevertheless, the energy transferred to the material per unit of radiation penetration (linear energy transfer) is lower. That means that deeper penetration culminates in lower energy transfer and, thus, lower absorption of dose rate. It is also important to note that e-beam penetration depth is inversely proportional to the material density and that the absorbed dose rate (kGy/s) is substantially higher than that observed for photons (kGy/h). That fact results in shorter irradiation periods to reach the same amount of energy absorbed.

Energy and current are essential parameters to be considered in the e-beam irradiation. The energy of the electrons establishes the depth penetration of an e-beam, and the e-beam current represents the number of electrons irradiating the material per unit of time. Thus, it is possible to control the amount and the rate of irradiation by changing its current. The atmosphere and temperature can also influence the irradiated materials. Regarding the first, irradiation in air atmosphere may cause oxidation of the sample by the contact of the reactive species formed with oxygen. Therefore, depending on the intention of the irradiation, this process may be avoided by sealing the material in a container with an inert atmosphere. In terms of temperature, an increase in the temperature is often observed due to the energy absorbed by the sample during irradiation. That will vary according to the specific heat of the material and the dose/dose rate. Temperature can also be suppressed by cooling the material during irradiation using an ice bath, or decreasing the dose/dose rate (Yoo, 2022).

In this work, we aimed to study the influence of parameters such as irradiation dose, buffer solution, and protein concentration on the synthesis of albumin nanoparticles by e-beam irradiation. Several syntheses

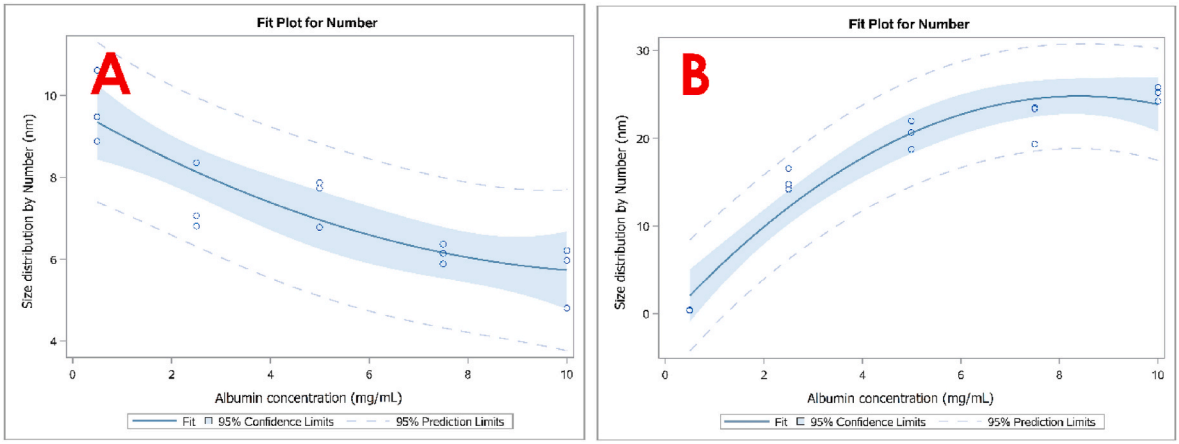

Fig. 7. Albumin nanoparticle size by number according to the albumin concentration (from 0.5 to 10 mg/mL) when the synthesis was performed under irradiation of (A) 5 kGy and (B) 25 kGy in phosphate buffer.

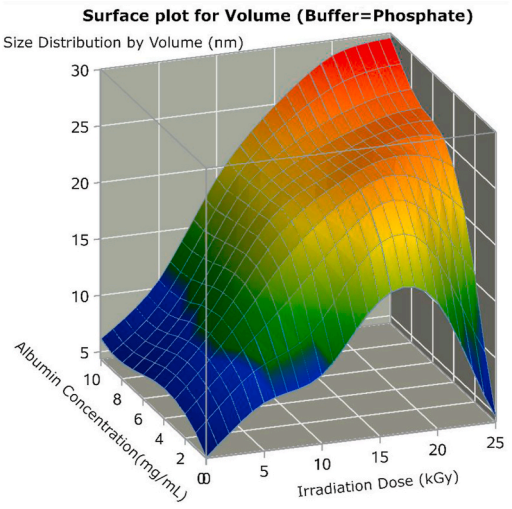

Fig. 8. Size by volume surface response plot for albumin nanoaparticles synthesized in phosphate buffer, varying protein concentration (from 0.5 to 10 mg/mL) and irradiation dose (from 1 to 25 kGy).

were carried out with two different buffers, namely phosphate or Tris-HCl, with five protein concentrations (0.5; 2.5; 5; 7.5; or 10 mg/mL), and six different irradiation doses (1; 5; 10; 15; 20; or 25 kGy). Results regarding size distribution were statistically evaluated to understand possible correlations among these variables.

2. Materials and methods

2.1. Materials

Bovine Serum Albumin (BSA, Heat shock fraction, purity ≥98%) was purchased from Sigma-Adrich (USA). Ethanol (EtOH), methanol (MeOH), anhydrous di- and monobasic phosphate, Tris base, and hydrochloric acid were acquired from Synth® (Brazil). All reagents were of analytical grade.

2.2. Preparation of albumin nanoparticles

The synthesis was performed in an ice bath using different concentrations of albumin (namely, 0.5, 2.5, 5, 7.5, and 10 mg/mL) dissolved in 50 mM phosphate (pH 7.4) or 50 mM Tris-HCl buffer (pH 7.6) containing 20% (v/v) ethanol and under an atmosphere of nitrous oxide. Samples were irradiated at 1, 5, 10, 15, 20, and 25 kGy in an e-beam irradiator (IPEN/CNEN-Brazil). E-beam energy was 1.44 MeV, current was 1.31 mA, pulse length was 100 cm, and dose rate was 5.35 kGy/s.

2.3. Characterization of the nanoparticles

2.3.1. Particle size distribution

Particle size distribution by means of intensity, number, and volume was determined by Dynamic Light Scattering (DLS), using a Litesizer 500 equipment (Anton Paar, Graz, Austria). Briefly, BSA-NPs samples were diluted 10 times in MilliQ water and analyzed using 10 runs of 10 s each and an angle of 173°. The values reported are the mean ± standard deviation of at least three different batches of nanoparticles.

2.4. Statistical analysis

A Fischer-Snedecor F test and a Kruskal-Wallis test were used to test the behavior between the buffers, verifying the need for stratification. The same techniques were applied to test the interaction between Albumin and Irradiation.

A multiple regression model was used with the response variable size distribution by: intensity, volume, and number, with the predictor variables Albumin and Irradiation, separated by type of buffer, according to the stratification tests. Response surface graphs (3D surface plots) and polynomial regression graphs were prepared when the interaction between Albumin and Irradiation was significant.

Robust statistics were used to establish the Outliers control parameter to reduce the impact of Outliers on regression models. The research team used a value limit of 100 for the three variables (Intensity, Number, and Volume) for the regression and robust regression analysis.

As all buffer comparisons showed a significant difference for all analyzed variables, it was decided to develop models of superficial response and inductive artificial intelligence for specific prediction for each buffer.

Unsupervised inductive machine learning was used for dimension reduction, the canonical variables tool of linear discriminant analysis, corroborated by non-parametric ANOVA and MANOVA tests.

Analyses were performed using SAS Studio (SAS Institute Inc, 2018) and Python (Pedregosa et al., 2011).

3. Experimental results

The complete model, factorial 2 × 5 × 6 (2 levels for Buffers, 5 levels for Albumin, and 6 levels for Irradiation), presented high significance for the Hydrodynamic Diameter variables (p-value <0.0001 for double and triple interaction). The triple interaction was deployed, and the

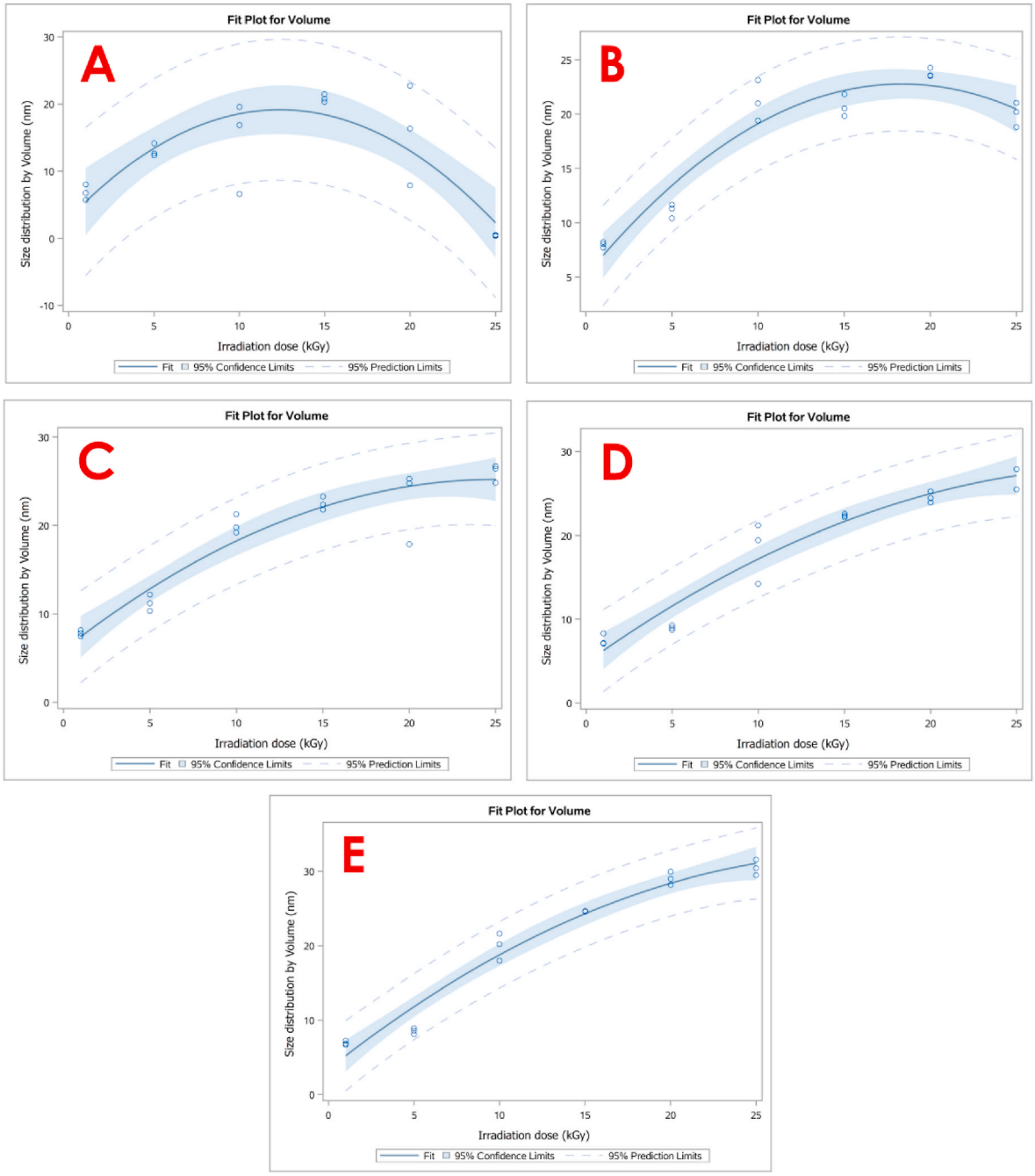

Fig. 9. Regressions plots correlating improvement of size by volume in function of irradiation dose (from 1 to 25 kGy) in phosphate buffer, under fixed protein concentration of (a) 0.5 mg/mL; (b) 2.5 mg/mL; (c) 5 mg/mL; (d) 7 mg/mL; (e) 10 mg/mL.

comparison between buffers was highly significant (p-value <0.0001), indicating that there was a need to perform separate analyses for each buffer. Size readings by Number (p-value <0.0001 for double and triple interaction) presented the same probabilistic results; size readings by intensity (p-value <0.007 for double interactions and p-value <0.0001 for triple interaction) also led to an unfolding of the buffers for the regression analyses. Finally, size readings by volume were similar to the hydrodynamic diameter.

In Fig. 1, 99% confidence ellipses without overlap can be observed for each buffer, with the buffer equality hypothesis test using NPManova (p-value <0.0001). Thus, the buffers showed highly significant statistical differences from a robust multivariate point of view. It can be observed that the most critical predictor variable to discriminate buffers was Numbers due to the smallest angle in relation to the ellipses, presenting high values for the TrisHCL buffer. The variables Intensity and Volume also showed high values for the TrisHCL buffer, but with less power of discrimination, indicated by the greater angulation of the vectors in the graph of the canonical variables. Even so, the three predictor variables showed highly significant differences in NPAnova (p-value<0.001).

Therefore, the unfolding of the triple interaction for surface plot and polynomial regression took place. The models with the highest importance for this research are presented in this topic. Linear regression analysis was performed for each buffer (Phosphate and Tris-HCl) considering fixed concentration or fixed dose rate. Responses with significance (or not) regarding size intensity, volume, and number were obtained and discussed in this section.

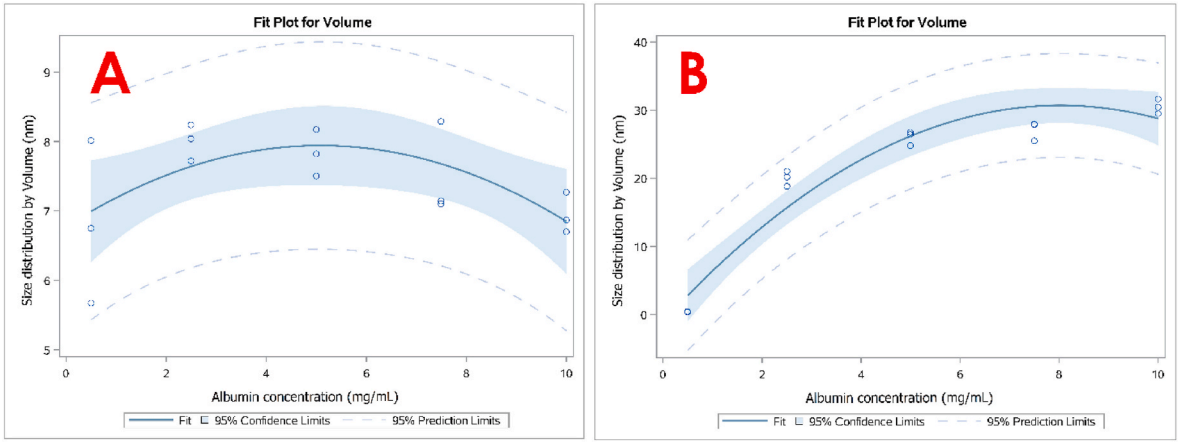

Fig. 10. Regressions plots correlating improvement of size by volume in function of protein concentration (from 0.5 to 10 mg/mL) in phosphate buffer, under fixed dose of irradiation of (a) 1 kGy and (b) 25 kGy.

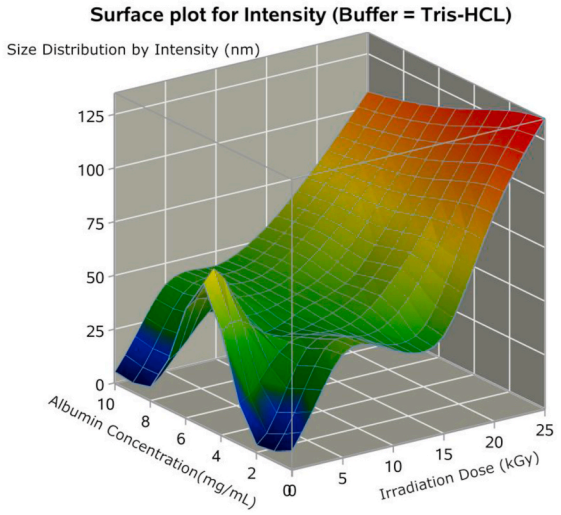

Fig. 11. Surface response plot for albumin nanoparticle size by means of intensity, for synthesis in TRIS buffer (pH 7.6), varying protein concentration (from 0.5 to 10 mg/mL) and irradiation dose (from 1 to 25 kGy).

3.1. Phosphate buffer synthesis

3.1.1. Size by intensity

When the nanoparticles were synthesized inphosphate buffer pH 7.4, the size results according to the irradiation dose and albumin concentration were not uniform. Nevertheless, the data point towards a dose-dependent nanoparticle size in most cases, especially with irradiation doses up to 15 kGy. The intensity results represent the size of the particles according to the reflected light, which means that the presence of bigger clusters, even if they are in smaller quantities, gain more emphasis. Thus, in Fig. 2, it is possible to observe a maximum size of 47 nm achieved by combining 8 mg/mL albumin concentration and 25 kGy irradiation dose. Bigger sizes (around 40 nm) were also observed for irradiation doses of 20 and 25 kGy combined with solution concentrations of 4 and 10 mg/mL.

On the other hand, the smaller particles obtained with lower irradiation doses (<10 kGy) presented clusters up to 20 nm. Additionally, 1 mg/mL albumin concentration combined with the irradiation dose (25 kGy) seemed to have a different response as small particles, up to 21 nm, were obtained. The graphic suggests that, for this amount of protein, there is a maximum size possible (around 30 nm) to be obtained with doses of 10 and 20 kGy. The same maximum was observed for the 10 mg/mL concentration at the irradiation dose of 10 kGy.

Based on these results, the hydrodynamic size of the nanoparticles (according to Intensity readings) in phosphate solution is mainly related to the dose of energy applied to the protein solution, as the higher the irradiation dose, the bigger the particles obtained. The concentration seemed to have more impact for irradiation doses of 20 and 25 kGy, when it was clear to see that the higher concentration (10 mg/mL) generated bigger particles (25 nm – size by number) and lower concentrations originated smaller ones (from 5 to 15 nm).

When maintaining the albumin concentration and varying the irradiation dose, the correlation of particle size by intensity according to the radiation dose was statistically significant in all albumin concentrations except for 0.5 mg/mL. As demonstrated in Fig. 3, the nanoparticle size increases with the radiation dose up to 20 kGy according to a linear regression model for albumin at 2.5 mg/mL, although only a low percentage of the data can be explained by this regression model (r-squared = 0.3613, $p < 0.0243$). There was a quadratic correlation between irradiation dose (up to 20 kGy) and particle size increase after albumin at 5.0 mg/mL was irradiated (r-squared = 0.6633, $p < 0.0095$). A similar correlation according to a quadratic regression model was found for albumin at 7.5 and 10 mg/mL, meaning that the hydrodynamic size increases when irradiation doses up to 15 kGy were used (r-squared = 0.5821 and $p < 0.0001$ for albumin at 7.5 mg/mL, and r-squared = 0.5951 and $p < 0.01$ for albumin at 10 mg/mL). The hydrodynamic size did not increase significantly with doses above 15 kGy in almost any of the albumin concentrations used for these experiments.

When the statistical analysis was performed with fixed irradiation dose and varying albumin concentration, a statistically significant correlation was only observed for 25 kGy, meaning that the nanoparticle size increases according to the increased albumin concentration, in consonant with the quadratic regression model (r-square = 0.4583; $p < 0.0268$) (Fig. 4). No statistical significance was found with the lower doses.

3.1.2. Size by number

The variation of size by number due to different albumin concentrations and irradiation doses, under fixed phosphate buffer, is demonstrated in Fig. 5. Size by number reveals the size of the majority of the particles in a given population. The graphic shows that bigger sizes (>25 nm) were obtained at higher doses of irradiation (>15 kGy) combined with higher concentrations of albumin (>8 mg/mL). The analysis suggests that the increase in irradiation dose has a higher impact on nanoparticle size than the albumin concentration. In lower irradiation doses (<10 kGy), the increased protein concentration did not result in a significant change in the size, with particles up to 10 nm. With 15 kGy, it was possible to observe an increase up to 15 nm when the

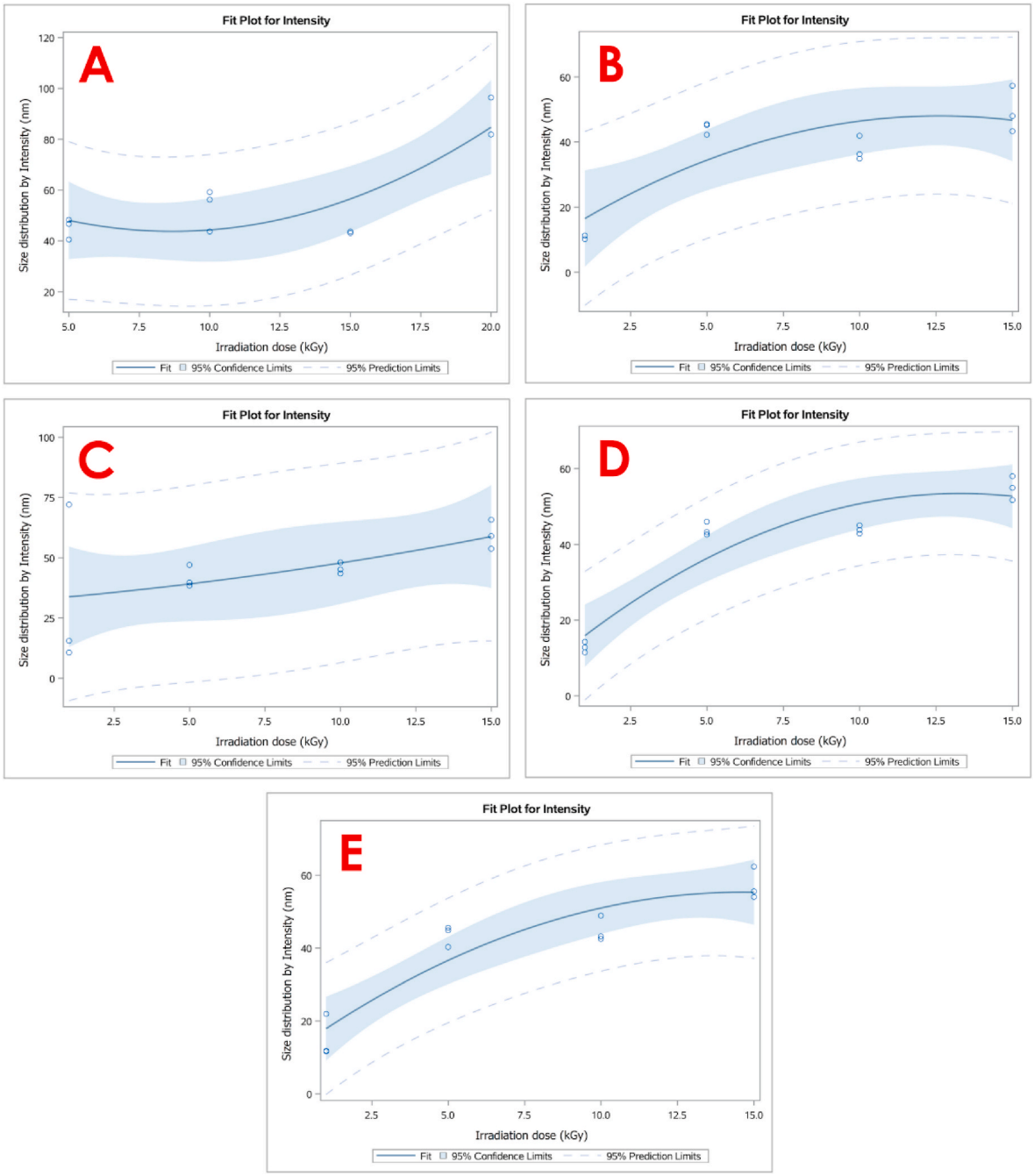

Fig. 12. Regression data of albumin nanoparticle size according to the irradiation dose (from 1 to 25 kGy) with fixed albumin concentrations of (A) 0.5 mg/mL, (B) 2.5 mg/mL, (C) 5.0 mg/mL, (D) 7.5 mg/mL, and (E) 10 mg/mL. Data for the synthesis in TRIS buffer.

concentration was increased to 10 mg/mL.

The linear regression analysis of size by number for fixed albumin concentrations (Fig. 6) revealed that, for all tested conditions, there is a correlation between dose of irradiation and nanoparticle hydrodynamic size. When albumin is fixed at 0.5 mg/mL and irradiated with e-beam in phosphate buffer, the number modification is statistically significant according to the concentration of albumin (r-squared = 0.637484), as demonstrated by the quadratic regression model ($p < 00.0001$). Therefore, the particle size increases as the irradiation dose increases until around 12 kGy, and with higher doses, it tends to stabilize and decrease.

When albumin is fixed at 2.5 mg/mL and irradiated with an e-beam in a phosphate buffer medium, the increase of hydrodynamic size by number is demonstrated by the quadratic regression model ($p < 0.0001$; r-squared = 0.8369). Therefore, the particle size increases as the irradiation dose increases until around 17 kGy, and with higher doses, it tends to stabilize and, then, decrease.

For other albumin concentrations (5, 7.5, and 10 mg/mL), linear regressions were more suitable to establish a correlation between size and irradiation dose. Therefore, in these conditions, it was observed that the particle hydrodynamic size increased by number as the irradiation dose was also increased up to 25 kGy.

Fixing albumin concentration and varying dose of irradiation disclosed a significant correlation for only two concentrations: 5 and 25 kGy (Fig. 7). When Albumin is irradiated with 5 kGy in a phosphate medium, the size by number modification presented statistical significance according to the concentration of albumin, although just a low percentage of the data can be explained by a linear regression model (p

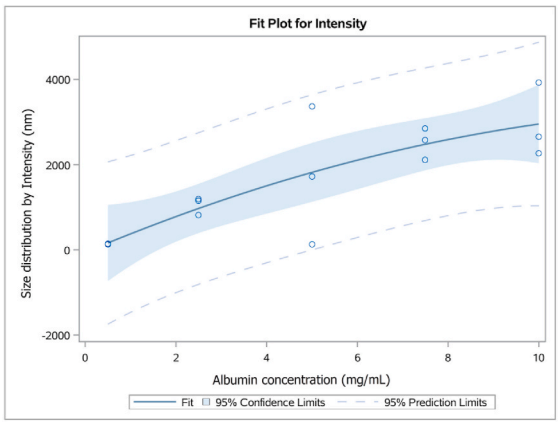

Fig. 13. Albumin nanoparticle size by means of intensity, according to the albumin concentration (from 0.5 to 10 mg/mL) when the synthesis was performed under irradiation with 25 kGy in TRIS buffer.

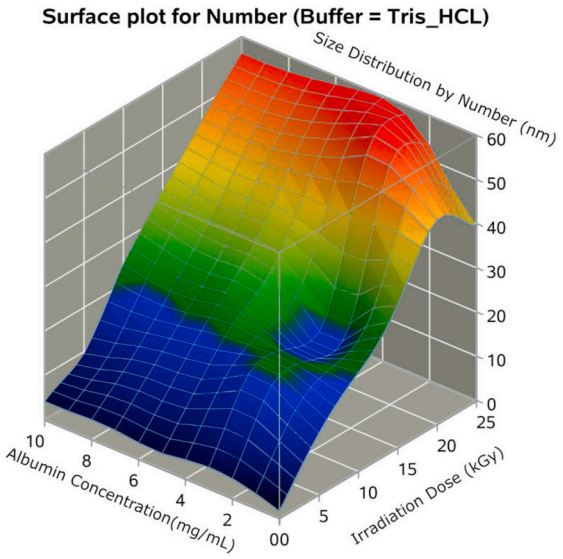

Fig. 14. Size by number surface response plot for albumin nanoparticles synthesized in Tris-HCl buffer, varying protein concentration (from 0.5 to 10 mg/mL) and irradiation dose (from 1 to 25 kGy).

= 0.0147; r-square = 0.3726). In this case, there was a decrease in particle hydrodynamic size as the albumin concentration was increased. On the other hand, for irradiation dose fixed at 25 kGy, the size by number variation was demonstrated by a quadratic regression model ($p < 0.0001$, r-square = 0.7447). Thus, in this case, it was observed that an augment in the protein concentration up to 7.5 mg/mL led to increased size by number, followed by a stabilization and, then, a decrease.

3.1.3. Size by volume

The response of nanoparticle sizes according to the volume measurement, i.e., considering the volume the particles occupy, is represented on the surface response plot in Fig. 8. The behavior observed is quite similar to the one observed in the response by number; however, a little increase in the hydrodynamic sizes is often obtained. The maximum size achieved in phosphate solution was 30 nm upon irradiation with 25 kGy in a 10 mg/mL albumin solution. In all concentrations, solutions irradiated with up to 5 kGy presented volume readings equal to number size, up to 10 nm. At 10 kGy, a slight increase in 0ize to 15 nm was reported, which was when compared to the values obtained by number. Therefore, it is clear that albumin concentration is likely to directly influence size augment, as bigger sizes were only obtained from more albumin-saturated solutions. Dose of irradiation could also affect this, but achieving a lower maximum limit for smaller protein concentrations.

Therefore, when albumin concentration is fixed and there is an analysis of how dose rate influences hydrodynamic size by volume, in general, an increase in size is observed according to the increase of irradiation dose, as demonstrated by quadratic regression models (Fig. 9). However, it is noted that for lower protein concentrations (0.5 mg/mL and 2.5 mg/mL), there was a limit at 12 and 17 kGy, respectively, to the size by volume increase ($p = <00.0001$, $r^2 = 0.6918$ and $p < 00.0001$, $r^2 = 0.8369$). Higher protein concentrations (5, 7.5, and 10 mg/mL) kept gaining size up to 25 kGy and had this limited at higher irradiation dose.

When irradiation dose was fixed and the increase of the protein concentration was evaluated concerning effects on size increase, the regression model was significant for 1, 5, and 25 kGy dose (Fig. 10). For 1 kGy and 25 kGy a quadratic model demonstrated that enhancing the BSA concentration also led to an increase in nanoparticles' hydrodynamic size by volume. In the first condition this was observed until 5 mg/mL, followed by a size decrease ($p = 0.0247$; $r^2 = 0.3143$). In the second one, augmented sizes were observed with albumin concentrations up to 7.5 mg/mL ($p = 0.0002$; $r^2 = 0.6992$). On the other hand, when the dose was fixed at 5 kGy, a linear regression model demonstrated a correlation of size decrease when protein concentration was increased.

3.2. Tris-HCl synthesis

3.2.1. Size by intensity

The DLS readings in terms of intensity are somewhat similar when it comes to the correlation between irradiation dose and albumin concentration in the final nanoparticle size. Overall, the main parameter influencing the nanoparticle size is the irradiation dose, whereas albumin concentration exerts influence on nanoalbumin size only with specific conditions. The buffer used for the synthesis, though, seems to be paramount to the outcomes.

When the nanoparticles were synthesized in Tris buffer with pH 7.6, the size results are more uniform according to the irradiation dose and albumin concentration (Fig. 11). The data reviews an irradiation dose-dependent nanoparticle size, especially with irradiation doses up to 10 kGy (see Fig. 12).

When the concentration of albumin was fixed and the irradiation dose was variable, the correlation of particle size according to the irradiation dose was statistically significant in all albumin concentrations. As demonstrated in Fig. 11, in summary, with 0.5 mg/mL of albumin, the nanoparticle hydrodynamic size increases with the irradiation dose up to 10 kGy according to a quadratic regression model (r-squared = 0.6450, $p < 0.0375$). There was a linear correlation between irradiation dose (up to 10 kGy) and particle size increase after albumin at 2.5 mg/mL was irradiated (r-squared = 0.5968, $p < 0.0203$), and a similar linear correlation was observed for all irradiation doses when albumin was irradiated at 5.0 mg/mL (r-squared = 0.5609, $p < 0.0009$). A similar correlation according to a quadratic regression model was found for albumin at 7.5 and 10 mg/mL, meaning that the nanoparticle size increases when irradiation doses up to 10 kGy were used (r-squared = 0.7771 and $p < 0.0094$ for albumin at 7.5 mg/mL, and r-squared = 0.7947 and $p < 0.0466$ for albumin at 10 mg/mL). The size did not increase significantly with doses above 10 kGy in almost all albumin concentrations used for these experiments.

When the statistical analysis was performed with fixed irradiation dose and varying albumin concentration, a statistically significant correlation was only observed for 25 kGy, meaning that the nanoparticle size increases with the increased albumin concentration, according to the quadratic regression model (r-square = 0.4091; $p < 0.0002$) (Fig. 13). No statistical significance was found with the lower doses.

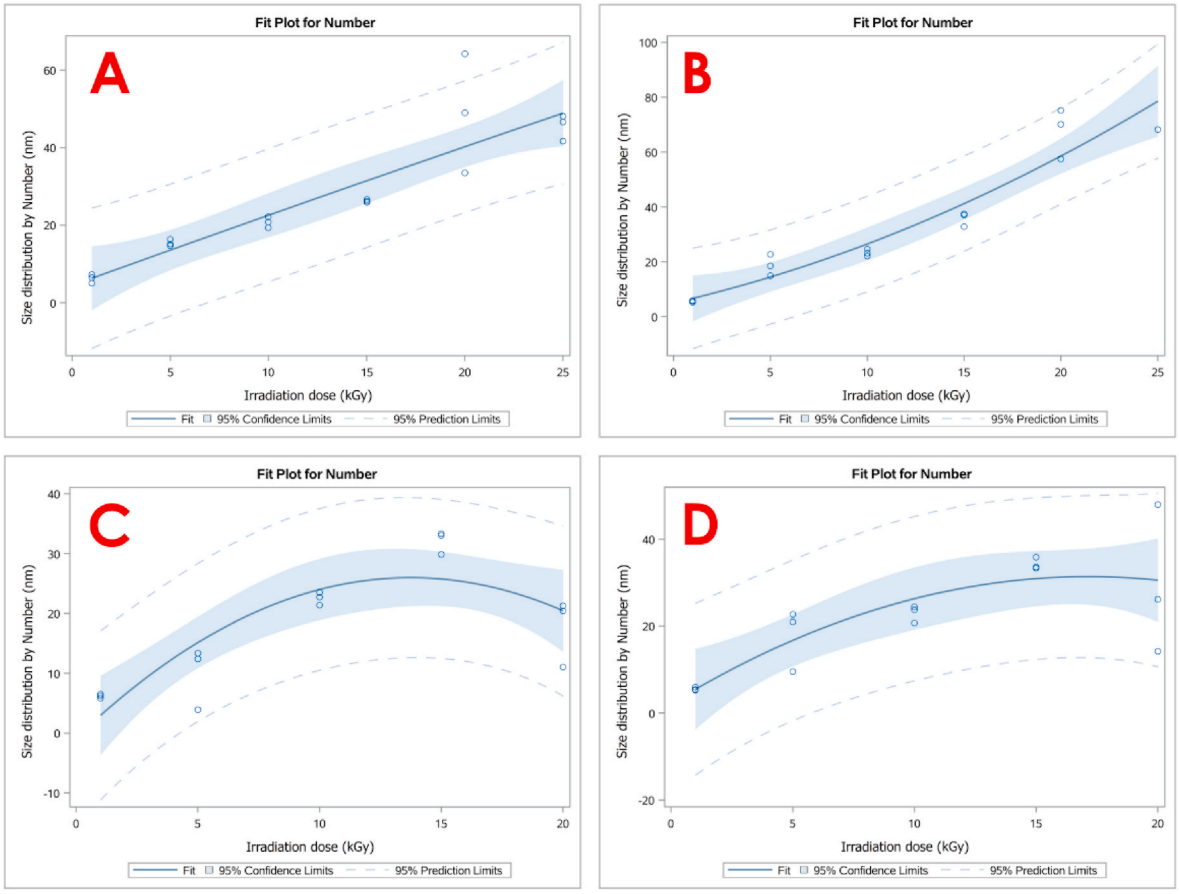

Fig. 15. Regression data of albumin nanoparticle size by number according to the irradiation dose (from 1 to 25 kGy) with fixed albumin concentrations of (A) 0.5 mg/mL, (B) 5 mg/mL, (C) 7.5 mg/mL, and (D) 10 mg/mL. Data for the synthesis in TRIS buffer.

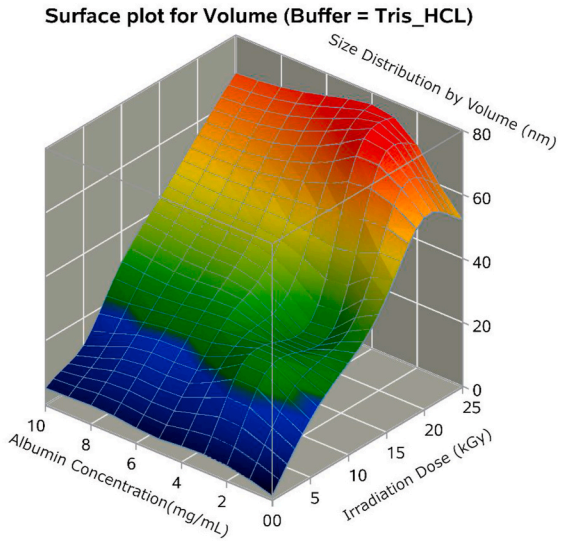

Fig. 16. Size by volume surface response plot for albumin nanoparticles synthesized in Tris-HCl buffer, varying protein concentration (from 0.5 to 10 mg/mL) and irradiation dose (from 1 to 25 kGy).

3.2.2. Size by number

In general, the synthesis in Tris HCl buffer produced bigger nanoparticles. As in phosphate experiments, it is observed the enhance of size particle mainly due to the increase of the energy applied as bigger sizes were again obtained in doses of 20 and 25 kGy. On Fig. 14, it is also observed a limit of size for low concentration (1 mg/mL) even with the application of high energy, however, considerably bigger particles (40 nm) are obtained here in comparison to the phosphate medium (5 nm). For concentrations from 5 mg/mL on, a common behavior is observed, with sizes up to 20 nm with doses up to 15 kGy; then ranging between 20 and 30 nm with 20 kGy; and achieving up to 60 nm with 25 kGy.

The regression models for these experiments revealed that when 0.5 mg/mL of albumin is irradiated with 1–25 kGy in Tris hydrochloride medium, the modification of hydrodynamic size by number is proportional to the e-beam irradiation dose increase, demonstrated by a linear regression models ($p < 0.0001$; $r^2 = 0.7581$). Similar behavior was observed for 5 mg/mL of BSA is irradiated with 1–25 kGy in Tris-HCl medium. However, the increase of size by number was better represented by a quadratic model ($p = 0.0103$, $r^2 = 0.6333$) - Fig. 15.

Quadratic models also fit better size growth behavior of HAS solutions at 7.5 mg/mL ($p = 0.0046$; $r^2 = 0.6139$) and 10 mg/mL ($p = 0.004$, $r^2 = 0.5908$). Howbeit, in these conditions a point of maximum growth was observed at lower irradiation dose: 14 kGy.

3.2.3. Size by volume

Volume results corroborate with size by number previously shown, with a slight increase up to 77 nm (Fig. 16). Again, it is likely that smaller sizes are obtained at lower irradiation doses and bigger ones for higher doses of energy (from 20 kGy on). Lower protein concentrations (up to 4 mg/mL) yielded smaller particles with doses up to 10 kGy, and in a range between 10 and 20 kGy, the particles presented the same size (around 20 nm). Between 20 and 25 kGy, another enhancement of the size is observed, but then, at 25 kGy, the size decreases again. Higher protein concentrations (from 5 mg/mL on) presented a continuous and proportional enhancement of particle size according to the increase of

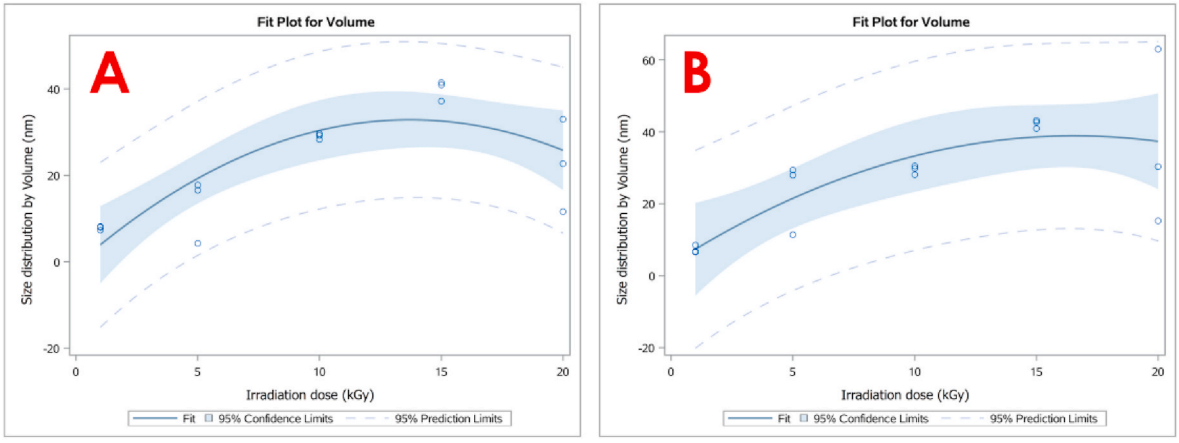

Fig. 17. Regressions plots correlating size improvement by volume in function of irradiation dose (from 1 to 25 kGy) in Tris-HCl buffer, under fixed protein concentration of (a) 7.5 mg/mL; (b) 10 mg/mL.

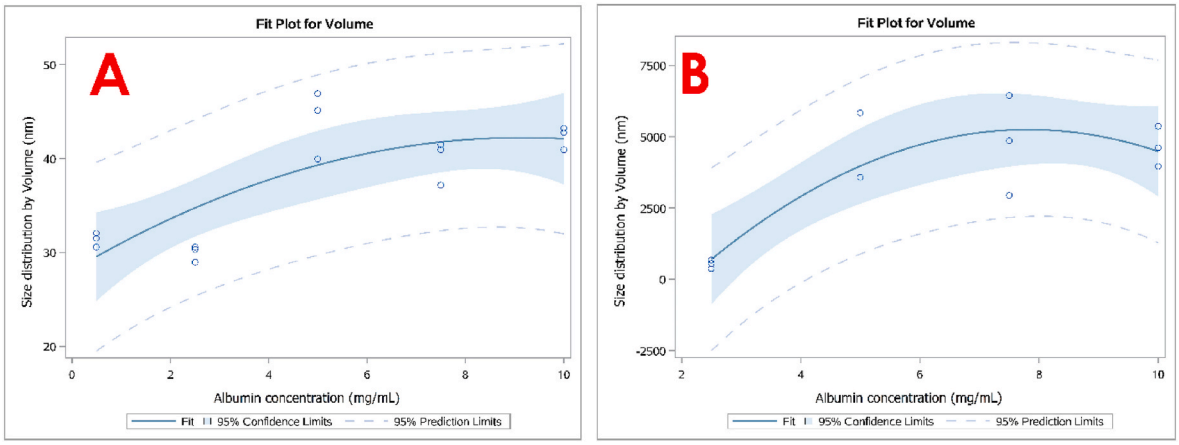

Fig. 18. Regressions plots correlating improvement of size by volume in function of protein concentration (from 0.5 to 10 mg/mL) in Tris-HCl buffer, under fixed dose of irradiation of (a) 15 kGy and (b) 25 kGy.

irradiation dose applied.

Considering regression models, Tris-HCl formulations presented a less frequent correlation between size by volume and irradiation dose (Fig. 17) or size by volume and concentration (Fig. 17). When protein concentration was fixed at 7.5 mg/mL, a quadratic model ($p = 0.0059$, $r^2 = 0.6271$) explained the correlation between dose and size: increasing the dose to 15 kGy caused augmented nanoparticles' size. Higher doses would cause a decrease in hydrodynamic size by volume in these conditions. However, the concentration fixed at 10 mg/mL fitted into a linear regression model ($p = 0.0245$; $r^2 = 0.5748$), with increased size by volume in accordance with the increase of irradiation dose.

When the irradiation dose was fixed, only two conditions could be fit into regression models: 15 and 25 kGy (Fig. 18). With a fixed dose of 15 kGy, a linear correlation ($p = 0.0268$; $r^2 = 0.5994$) was observed: the higher the concentration, the bigger the size of the nanoparticles by volume. At 25 kGy, a quadratic model ($p = 0.0253$; $r^2 = 0.6800$) revealed that size increased up to a 7.5 mg/mL concentration, and then, a decrease of the size was observed mediated by concentration increase.

4. Discussion

The radiation-induced intramolecular crosslinking method, first developed by Ulansky and Rosiak, has been demonstrated to be a very suitable pathway to obtain protein nanoparticles. Radio-induced synthesis of nanoparticles made of gelatin, albumin and papain have been previously reported in the literature by different groups. The main crosslinking mechanism of HSA nanoparticles via high energy irradiation is the formation of bityrosines, in which the oxidizing species originated by water radiolysis, such as hydroxyl radicals, allow the formation of Tyr-Tyr bonds (Achilli et al., 2015; Queiroz et al., 2016; G. H.C. Varca et al., 2016). In this work it was also possible to observe that the irradiated albumin presented higher bityrosin sign when compared to the native protein (Supplementary material), and that, the higher the dosed, higher the bityrosin levels. As nanoparticles were obtained by means of e-beam irradiation, an experimental design was done in order to study the ideal parameters to prepare these nanoparticles. The functionality and stability of a protein depends on parameters such as pH, temperature, and ionic strength of the aqueous medium. Because of that, proteins are usually studied in buffer solutions in order to maintain their structure and activity. However, it is important to point out that not all the buffers interact with proteins in the same way. The buffer may selectively bind to the native or denatured state of the protein and affect the microenvironment or water shell around the biomacromolecule (Satish et al., 2017). By tabulating all the regression results discussed on topic 3, it is possible to have an overview of the influence of variables BSA concentration and irradiation dose, according to the buffer used as media (Table 1). Concerning the protein concentration, radiation seemed to influence nanoparticle size for all fixed concentrations. For phosphate buffer synthesis, there was a linear correlation in terms of size by number related to the bigger population in a sample, from 5 to 10 mg/mL. On the other hand, for the same concentration range, sizes by volume and intensity presented a quadratic correlation, suggesting that

Table 1
Data obtained by statistical analysis concerning the correlation between BSA concentration and size (I-intensity, N-number, and V-volume) or irradiation dose and size. The gray cells indicate if the correlation is linear or quadratic (quadr.).

Fixed variable		PBS		Tris HCl	
		Linear	Quadr.	Linear	Quadr.
BSA 0.5 mg/mL	I				
	N				
	V				
BSA 2.5 mg/mL	I				
	N				
	V				
BSA 5 mg/mL	I				
	N				
	V				
BSA 7.5 mg/mL	I				
	N				
	V				
BSA 10 mg/mL	I				
	N				
	V				
1 kGy	I				
	N				
	V				
5 kGy	I				
	N				
	V				
10 kGy	I				
	N				
	V				
15 kGy	I				
	N				
	V				
20 kGy	I				
	N				
	V				
25 kGy	I				
	N				
	V				

in these conditions, there is a maximum limit to nanoparticle growth. When protein concentration is fixed, the higher the energy dose, the bigger the nanoparticles. The growth limit may be related to the availability of protein molecules as, at some point, they all may be crosslinked and, maybe, far enough from each other not to initiate new interactions. Moreover, it is important to mention the well-established scavenger properties of ethanol that, in the process, decrease the amount of radicals available to interact with the protein. The presence of ethanol also implies that by desolvating the protein(altering the solvation layer around the molecules), suitable proximity of protein molecules is provided, inducing intermolecular interactions (Varca et al., 2016).

When dose irradiation is fixed, it is only possible to see a more critical correlation between size and protein concentration at 25 kGy dose. This correlation is described by a quadratic model for the three aspects of size. It implies concentrations do not necessarily play an important role in nanoparticle formation at fixed dose irradiation, except at 25 kGy. In this situation, there would also be a limit of protein concentration to cause the augment of size, maybe because of a restriction of intermolecular interactions as several small nuclei are formed by the high energy applied.

For Tris HCl buffer, similar behavior is observed regarding more influence of irradiation dose than protein concentration. For fixed concentrations of 7.5 and 10 mg/mL, quadratic models showed a correlation between size and irradiation dose, except for size by volume in the second condition, in which the correlation was linear. Thus, mainly at these two fixed concentrations, a size growth is observed by the irradiation dose increase. However, as observed for formulation in phosphate medium, Tris HCl synthesis also requires a minimum of 25 kGy dose to present a correlation between the nanoparticles size augment and protein concentration.

Therefore, it can be stated that radiation plays a more important role in nanoparticle size. Even though this mostly happens within some fixed concentration limits: between 2.5 and 10 mg/mL for phosphateand between 7.5 and 10 mg/mL for Tris HCl medium. Both formulations presented concentration and size correlation only at 25 kGy fixed dose.

Varca and coworkers have done several studies in the past, mainly to evaluate the influence of cosolvent and dose irradiation over protein nanoparticle size. In The case of papain, it was observed that the irradiation dose effect on nanoparticle size was negligible, while the desolvation provided by ethanol was crucial. However, BSA seems to respond differently, probably undergoing distinct crosslinking mechanisms and presenting size modification upon varying irradiation doses. One of the hypotheses mentioned by the authors is that the presence of methionine and more disulfide bonds in albumin could allow other pathways for nanoparticle formation in addition to the bityrosine pathway (Fazolin et al., 2018; Queiroz et al., 2016; Gustavo H.C. Varca et al., 2016; Varca et al., 2014).

Queiroz et al. (2016) demonstrated that the irradiation of BSA with a 10 kGy dose, and in the absence of ethanol, could generate nanoparticles, increasing protein size from 6.6 ± 0.3 nm to 16.6 ± 2.3 nm. The aim of adding a desolvating agent was to solubilize hydrophobic or poorly soluble drugs, looking forward to a drug-loading process. As mentioned before, the main effect of ionizing radiation on the nanoparticles synthesis in aqueous solution, is the formation of oxidizing species such as hydroxyl radicals as a result of water radiolysis that will contribute to the protein crosslinking via bityrosines formation. Other linkages, such as Cys-Cys via disulfide bonds, may also occur. Added to that, SDS-PAGE performed in the same study, proved an intermolecular crosslinking as molecular weight augmented from 66 kDa to 270 kDa after irradiation.

The study about BSA nanoparticles synthesis via γ-irradiation concluded that the best parameters were a dose of 10 kGy (at dose rate of 5 kGy/h), protein concentration of 12.5 mg/mL, and 20% (v/v) of ethanol content (Varca et al., 2016). Our study agrees with the literature, as radiation seems to have a great influence on the size of BSA nanoparticles. Also, this work revealed that protein concentration will only interfere in higher irradiation doses such as 25 kGy.

Concerning surface response plots, they corroborate to the described in the literature as smaller protein concentrations generate smaller nanoparticles, even though it wasn't possible to observe in the regression analysis. Also, these plots disclose a more proportional size growth according to protein concentration and irradiation dose when Tris HCl media was used.

5. Conclusions

Based on the surface response plots obtained from the triple interaction (irradiation dose x albumin concentration x size), smaller protein concentrations consistently lead to smaller particles for both buffers used. This observation aligns with data reported in the literature, as the distance between molecules in the solution induces intramolecular crosslinks and prevents aggregations. However, smaller particles are

obtained in phosphate solutions at these lower concentrations, while in Tris-HCl medium, nanoparticle sizes can reach up to 125 nm as the irradiation dose increases. It was also observed that in Tris-HCl media, particle growth was more proportional to the increase in concentration and irradiation dose within the parameters studied, likely presenting a maximum point at doses higher than 25 kGy. The quadratic regression correlations found may confirm the presence of a maximum point for the experiments conducted in the Tris-HCl buffer. Considering all the data described the synthesis in Tris-HCl buffer is the most suitable option. This is because it leads to more homogeneous size control in accordance with the irradiation dose and albumin concentration. Additionally, a maximum size can be achieved with a lower irradiation dose compared to the synthesis performed in phosphate buffer (maximum size achieved at 10 kGy in Tris-HCl buffer versus 15 kGy in phosphate buffer).

CRediT authorship contribution statement

Aryel H. Ferreira: Conceptualization, Data curation, Formal analysis, Investigation, Methodology, Project administration, Validation, Visualization, Writing – original draft, Writing – review & editing. **Caroline S.A. Lima:** Conceptualization, Data curation, Formal analysis, Investigation, Methodology, Validation, Visualization, Writing – original draft, Writing – review & editing. **Cassia Priscila Cunha da Cruz:** Investigation, Methodology. **Lucas F. Freitas:** Data curation, Validation, Visualization, Writing – original draft, Writing – review & editing. **Gustavo N. Furlan:** Data curation, Formal analysis, Software, Validation. **Robson C. de Lima:** Data curation, Formal analysis, Software, Validation, Visualization. **Gabriel Adrián Sarriés:** Data curation, Formal analysis, Software, Validation, Visualization. **Ademar B. Lugão:** Conceptualization, Formal analysis, Project administration, Supervision.

Declaration of competing interest

The authors declare that they have no known competing financial interests or personal relationships that could have appeared to influence the work reported in this paper.

Data availability

Data will be made available on request.

Appendix A. Supplementary data

Supplementary data to this article can be found online at https://doi.org/10.1016/j.radphyschem.2024.111974.

References

Achilli, E., Casajus, G., Siri, M., Flores, C.Y., Kadłubowski, S., Alonso, S. del V., Grasselli, M., 2015. Preparation of protein nanoparticle by dynamic aggregation and ionizing-induced crosslinking. Colloids Surfaces A Physicochem. Eng. Asp. 486, 161–171. https://doi.org/10.1016/j.colsurfa.2015.09.047.

Čubová, K., Čuba, V., 2020. Synthesis of inorganic nanoparticles by ionizing radiation – a review. Radiat. Phys. Chem. 169, 108774 https://doi.org/10.1016/j.radphyschem.2020.108774.

Elzoghby, A.O., Samy, W.M., Elgindy, N.A., 2012. Albumin-based nanoparticles as potential controlled release drug delivery systems. J. Contr. Release. https://doi.org/10.1016/j.jconrel.2011.07.031.

Fanali, G., Di Masi, A., Trezza, V., Marino, M., Fasano, M., Ascenzi, P., 2012. Human serum albumin: from bench to bedside. Mol. Aspect. Med. 33, 209–290. https://doi.org/10.1016/j.mam.2011.12.002.

Farjadian, F., Ghasemi, A., Gohari, O., Roointan, A., Karimi, M., Hamblin, M.R., 2019. Nanopharmaceuticals and nanomedicines currently on the market: challenges and opportunities. Nanomedicine. https://doi.org/10.2217/nnm-2018-0120.

Fazolin, G.N., Varca, G.H.C., Kadlubowski, S., Sowinski, S., Lugão, A.B., 2018. The effects of radiation and experimental conditions over papain nanoparticle formation: towards a new generation synthesis. Radiat. Phys. Chem. 169 https://doi.org/10.1016/j.radphyschem.2018.08.033.

Jain, A., Singh, S.K., Arya, S.K., Kundu, S.C., Kapoor, S., 2018. Protein nanoparticles: promising platforms for drug delivery applications. ACS Biomater. Sci. Eng. 4, 3939–3961. https://doi.org/10.1021/acsbiomaterials.8b01098.

Lohcharoenkal, W., Wang, L., Chen, Y.C., Rojanasakul, Y., 2014. Protein nanoparticles as drug delivery carriers for cancer therapy. BioMed Res. Int. https://doi.org/10.1155/2014/180549.

Parodi, A., Miao, J., Soond, S.M., Rudzińska, M., Zamyatnin, A.A., 2019. Albumin nanovectors in cancer therapy and imaging. Biomolecules 9. https://doi.org/10.3390/biom9060218.

Pedregosa, F., Varoquaux, G., Gramfort, A., Michel, V., Thirion, B., Grisel, O., Blondel, M., Müller, A., Nothman, J., Louppe, G., Prettenhofer, P., Weiss, R., Dubourg, V., Vanderplas, J., Passos, A., Cournapeau, D., Brucher, M., Perrot, M., Duchesnay, 2011. Scikit-learn: machine learning in Python. J. Mach. Learn. 12 https://doi.org/10.48550/arXiv.1201.0490.

Queiroz, R.G., Varca, G.H.C., Kadlubowski, S., Ulanski, P., Lugão, A.B., 2016. Radiation-synthesized protein-based drug carriers : size-controlled BSA nanoparticles. Int. J. Biol. Macromol. 85, 82–91.

Remita, H., Lampre, I., Mostafavi, M., Balanzat, E., Bouffard, S., 2005. Comparative study of metal clusters induced in aqueous solutions by γ-rays, electron or C6+ ion beam irradiation. Radiat. Phys. Chem. 72, 575–586. https://doi.org/10.1016/j.radphyschem.2004.03.042.

SAS Institute Inc, 2018. SAS Studio [software] [WWW Document]. URL, Version 3.8. https://www.sas.com/pt_br/software/studio.html.

Satish, L., Millan, S., Das, S., Jena, S., Sahoo, H., 2017. Thermal aggregation of bovine serum albumin in conventional buffers: an insight into molecular level interactions. J. Solut. Chem. 46, 831–848. https://doi.org/10.1007/s10953-017-0612-0.

Soto Espinoza, S.L., Sánchez, M.L., Risso, V., Smolko, E.E., Grasselli, M., 2012. Radiation synthesis of seroalbumin nanoparticles. Radiat. Phys. Chem. 81, 1417–1421. https://doi.org/10.1016/j.radphyschem.2011.11.040.

Varca, G.H.C., Ferraz, C.C., Lopes, P.S., Mathor, M. beatriz, Grasselli, M., Lugão, A.B., 2014. Radio-synthesized protein-based nanoparticles for biomedical purposes. Radiat. Phys. Chem. 94, 181–185. https://doi.org/10.1016/j.radphyschem.2013.05.057.

Varca, G.H.C., Kadlubowski, S., Wolszczak, M., Lugão, A.B., Rosiak, J.M., Ulanski, P., 2016. Synthesis of papain nanoparticles by electron beam irradiation – a pathway for controlled enzyme crosslinking. Int. J. Biol. Macromol. 92, 654–659. https://doi.org/10.1016/j.ijbiomac.2016.07.070.

Varca, Gustavo H.C., Queiroz, R.G., Lugão, A.B., 2016. Irradiation as an alternative route for protein crosslinking: cosolvent free BSA nanoparticles. Radiat. Phys. Chem. 124, 111–115. https://doi.org/10.1016/J.RADPHYSCHEM.2016.01.021.

Verma, D., Gulati, N., Kaul, S., Mukherjee, S., Nagaich, U., 2018. Protein based nanostructures for drug delivery. J. Pharm. (Lahore) 2018, 1–18. https://doi.org/10.1155/2018/9285854.

Yoo, S.H., 2022. Short review of utilization of electron-beam irradiation for preparing polyacrylonitrile-based carbon fibers and improving properties of carbon-fiber-reinforced thermoplastics. Carbon Lett 32, 413–429. https://doi.org/10.1007/s42823-021-00304-8.

Zolle, U., 2007. Technetium-99m pharmaceuticals: preparation and quality control in nuclear medicine. In: Technetium-99m Pharmaceuticals: Preparation and Quality Control in Nuclear Medicine. Springer Berlin Heidelberg. https://doi.org/10.1007/978-3-540-33990-8.